ChemComm

COMMUNICATION

View Article Online
View Journal | View Issue

Cite this: *Chem. Commun.*, 2024, **60**, 12912

Received 22nd August 2024,
Accepted 7th October 2024

DOI: 10.1039/d4cc04296d

rsc.li/chemcomm

Cationic dinuclear complexes $[M_2(PCP)_2\mu\text{-}Cl][GaCl_4]$ of the group 10 elements. metallophilic interactions and catalytic dehydrogenation of Me_2NHBH_3†

Fabio Meyer, Pim Puylaert, Daniel Duvinage, Emanuel Hupf * and Jens Beckmann *

The facile synthesis of the cationic dinuclear group 10 complexes $[M_2(PCP)_2\mu\text{-}Cl]^+$ (M = Ni, Pd, Pt) by transmetallation from a simple Ga precursor is reported (PCP = 2,6-$(Ph_2P)C_6H_3$). Their use for the catalysed dehydrogenation of Me_2NHBH_3 shows that Ni has a higher reactivity than Pt, whereas Pd is inactive.

The stability of organometallic species relies essentially on a judicious choice of ligands and substituents, which provide kinetic and electronic stabilization to the metal atom. For this purpose, bidentate 2-diorganophosphinophenyl carbanions, $[2\text{-}R_2PC_6H_4]^-$ (**I**, R = Ph, *i*-Pr) are frequently employed for a large number of main group and transition metal complexes (Fig. 1).[1] Recently, we introduced the related bis(2,6-diphenylphosphino)phenyl carbanion, $[2,6\text{-}(Ph_2P)_2C_6H_3]^-$ (**II**),[2] as a tridentate "PCP" ligand, which is also isoelectronic with the previously known neutral bis(2,6-diphenylphosphino)pyridine, $2,6\text{-}(Ph_2P)_2C_5H_2N$ (**III**), ligand (Fig. 1).[3] So far, the PCP ligand was applied for the preparation of photoactive coinage metal complexes, $[Cu_4(PCP)_3]^+$,[4] and linear and cyclic $[Au_4(PCP)_2(tht)_2]^{2+}$, as well as a mixed-metal pincer complex, *e.g.* $HgAu_2(PCP)Cl_3$.[2] In an effort to broaden the scope of the PCP ligand towards main group chemistry, we have now reacted the lithium reagent $2,6\text{-}(Ph_2P)_2C_6H_3]_2Li$[5] with $GaCl_3$ to give rise to the formation of $[2,6\text{-}(Ph_2P)_2C_6H_3]_2GaCl$ (**1**), which was isolated as colourless crystals in 95% yield (Scheme 1).

Notably, variations of the stoichiometric ratio did not give the mono- or trisubstituted Ga-species in significant amounts. The molecular structure of **1** shows that only one of the four P atoms is engaged in the first coordination sphere of the Ga atom (Fig. 2). The spatial arrangement may thus be described as distorted tetrahedral. The primary Ga–P bond length of **1** (2.567(1) Å) is substantially shorter than the remaining secondary Ga–P contacts (3.071(5), 3.382(5), 3.653(7) Å), which, however, are still within the van der Waals limit (4.2 Å). In solution, the P atoms are equivalent on the NMR time scale at room temperature, as the ^{31}P NMR spectrum ($CDCl_3$) of **1** shows only one signal at $\delta = -3.0$ ppm. No qualitative change was observed at −30 °C. With the aim to prepare Ga-based Z-type complexes,[6] we reacted

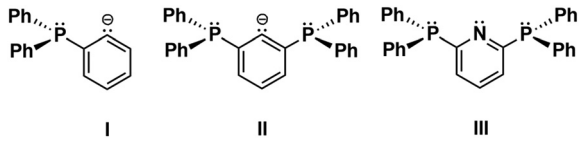

Fig. 1 Bi- and tridentate P-based ligands.

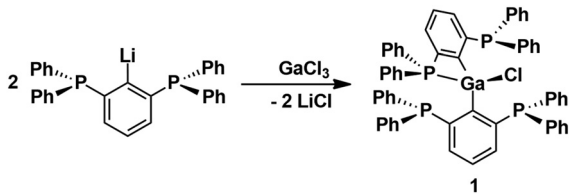

Scheme 1 Synthesis of **1**.

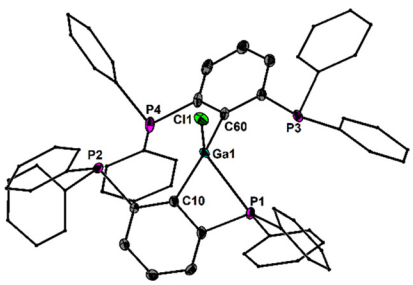

Fig. 2 Molecular structure of **1** showing 50% probability ellipsoids and the atomic numbering scheme. Selected bond lengths: Ga1–C10 1.975(2), Ga1–C60 1.994(2), Ga1–Cl1 2.250(1), Ga1–P1 2.567(1) Å.

Institute für Anorganische Chemie und Kristallographie, Universität Bremen, Leobener Str. 7, 28359 Bremen, Germany. E-mail: hupf@uni-bremen.de, j.beckmann@uni-bremen.de

† Electronic supplementary information (ESI) available: M = Ni, Pd, Pt. PCP = 2,6-bis(diphenylphosphino)phenyl. CCDC 2378087–2378091. For ESI and crystallographic data in CIF or other electronic format see DOI: https://doi.org/10.1039/d4cc04296d

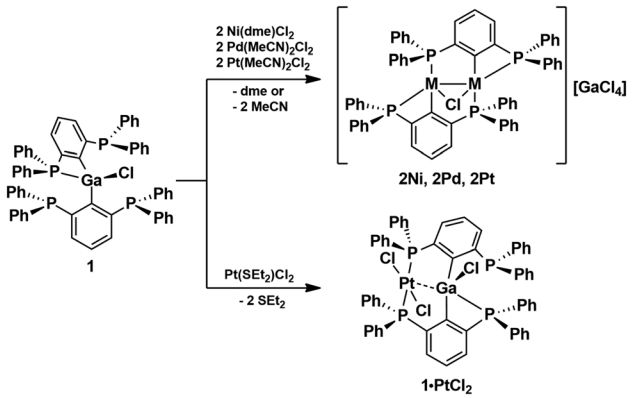

Scheme 2 Synthesis of **2M** (M = Ni, Pd, Pt) and complexation reaction to give **1**·$PtCl_2$.

1 with two equivalents of $Ni(dme)Cl_2$, $Pd(MeCN)_2Cl_2$ and $Pt(MeCN)_2Cl_2$, respectively. Surprisingly, in all cases rapid transmetallation occurred and the cationic dinuclear group 10 complexes[7] $[M_2(PCP)_2\mu\text{-Cl}][GaCl_4]$ (**2M**, M = Ni, Pd, Pt; PCP = 2,6-$(Ph_2P)_2C_6H_3$) formed, which were isolated as red, orange and red crystals in 92%, 72% and 64% yield, respectively (Scheme 2). The molecular structures of **2Ni**, **2Pd** and **2Pt** reveal complete separation of the $[M_2(PCP)_2\mu\text{-Cl}]^+$ cations and the $[GaCl_4]^-$ anions, which formed from the expelled Ga(iii) ions of **1** (Fig. 3). The spatial arrangement of the metal atoms is distorted square planar and defined by *cis*-P_2CCl donor sets. The two metal atoms in the dinuclear motifs are bridged by the Cl atoms. The M–M distances of **1Ni** (2.713(1) Å), **1Pd** (2.807(1) Å) and **1Pt** (2.818(1) Å) are indicative of metallophilic interactions[8] and increase with the atomic number of the group 10 metals.

The outer P atoms of the structural motifs are situated in *trans*-position of the Cl atoms, whereas the inner P atoms are located in *trans*-position of the C atoms. The outer M–P bond lengths of **2Ni** (2.141(1), 2.149(1) Å), **2Pd** (2.236(2), 2.252(2) Å) and **2Pt** (2.222(1), 2.227(1) Å) are generally shorter than the inner M–P bond lengths of **2Ni** (2.230(1), 2.232(1) Å), **2Pd** (2.354(2), 2.360(2) Å) and **2Pt** (2.330(1), 2.334(1) Å), which is consistent with the larger *trans*-effect of the Pt–C bond compared to the Pt–Cl bond.[9] The fact that the respective Pt–P bond lengths are shorter than the Pd–P bonds is attributed to the relativistic contraction of the 6s orbital of Pt.[8] The ^{31}P NMR spectra ($CDCl_3$) of **2Ni**, **2Pd**, **2Pt** show two distinctively different signals of equal intensity, which suggests that the molecular structures are retained in solution. The less shielded signals of **2Ni** (δ = 9.2 ppm), **2Pd** (δ = 8.2 ppm) and **2Pt** (δ = 13.0 ppm) are assigned to the inner P atoms, whereas the more shielded signals of **2Ni** (δ = −60.5 ppm), **2Pd** (δ = −76.3 ppm) and **2Pt** (δ = −76.1 ppm) belong to the outer P atoms. The assignment is based on the observed $^1J(^{31}P–^{123}Pt)$ couplings of **1Pt** of the inner (2073 Hz) and outer (4081 Hz) P atoms under the assumption that the magnitude inversely correlates with the bond lengths. The reaction of **1** with a different Pt-source, namely, $Pt(Et_2S)_2Cl_2$, in an equimolar ratio, indeed afforded the Z-type complex **1**·$PtCl_2$, which was isolated as pale yellow crystals in 59% yield (Scheme 2). Attempts to prepare similar Ni and Pd complexes failed and gave only **2Ni** and **2Pd** as principal products.

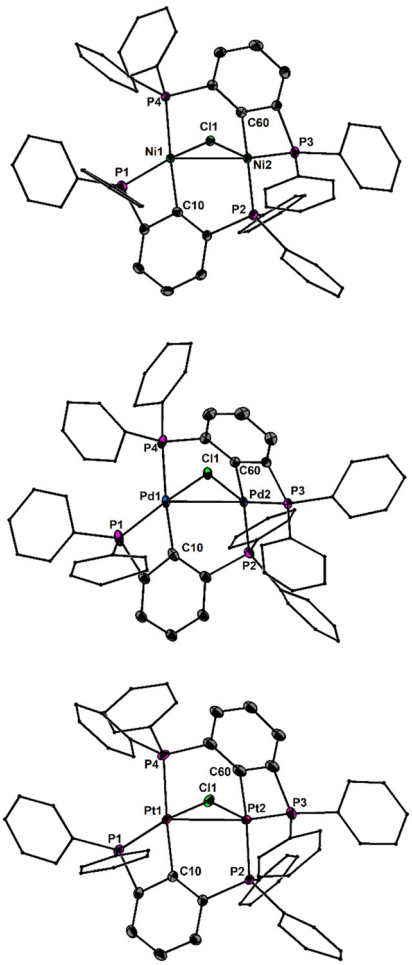

Fig. 3 Molecular structures of **2Ni** (top), **2Pd** (middle) and **2Pt** (bottom) showing 50% probability ellipsoids and the atomic numbering scheme. Selected bond lengths of **2Ni**: Ni1–C10 1.925(2), Ni1–Cl1 2.247(1), Ni1–P1 2.149(1), Ni1–P4 2.232(1), Ni2–C60 1.910(2), Ni2–Cl1 2.219(1), Ni2–P2 2.230(1), Ni2–P3 2.141(1), Ni1–Ni2 2.713(1) Å. Selected bond lengths of **2Pd**: Pd1–C10 2.042(8), Pd1–Cl1 2.396(2), Pd1–P1 2.252(2), Pd1–P4 2.360(2), Pd2–C60 2.052(5), Pd2–Cl1 2.415(2), Pd2–P2 2.354(2), Pd2–P3 2.236(2), Pd1–Pd2 2.807(1) Å. Selected bond lengths of **2Pt**: Pt1–C10 2.040(2), Pt1–Cl1 2.448(1), Pt1–P1 2.222(1), Pt1–P4 2.334(1), Pt2–C60 2.032(2), Pt2–Cl1 2.418(1), Pt2–P2 2.330(1), Pt2–P3 2.227(1), Pt1–Pt2 2.818(1) Å.

The molecular structure of **1**·$PtCl_2$ confirms the putative square planar arrangement of the Pt atoms, which adopts a *cis*-configuration of the two P atoms (Fig. 4). The Ga atom is situated perpendicular to Pt square plane. The Pt–Ga bond length (3.078(1) Å) suggests that the occupied dz^2 orbital at the Pt atom tentatively donates electron density to the vacant orbital at the Ga atom suggesting Z-type coordination. The Ga–P bond length of **1**·$PtCl_2$ (2.543(1) Å) is shorter than in the parent **1** (2.567(1) Å). The ^{31}P NMR spectrum ($CDCl_3$, 243 K) of **1**·$PtCl_2$ shows four equally intense signals. The two more deshielded signals at δ = 30.8 and 24.7 showing $^1J(^{31}P–^{123}Pt)$ couplings of 3430 Hz and 3016 Hz and are assigned to the P atoms involved in the coordination to the Pt atom. The two

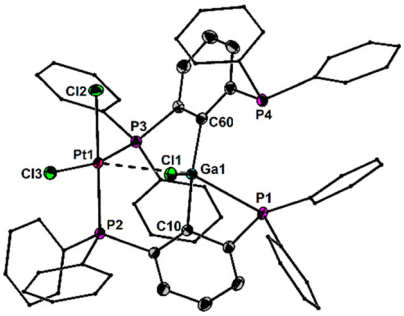

Fig. 4 Molecular structure of **1**·$PtCl_2$ showing 50% probability ellipsoids and the atomic numbering scheme. Selected bond lengths: Ga1–C10 2.009(2), Ga1–C60 1.994(2), Ga1–Cl1 2.190(1), Ga1–P1 2.543(1), Pt1–Cl2 2.359(1), Pt1–Cl3 2.337(1), Pt1–P2 2.258(1), Pt1–P3 2.251(1), Pt1–Ga1 3.078(1) Å.

more shielded signals are doublets centred at δ = −1.7 and −10.1 ppm both showing the same $J(^{31}P–^{31}P)$ couplings (102 Hz), which are indicative for through space interactions[10] of the two remaining P atoms *via* their electron lone pairs. This is quite unexpected in light of the large P···P distance (3.731(9) Å).

The most interesting structural feature of the cations **2M** (M = Ni, Pd, Pt) are the metallophilic interactions, which were analyzed in more detail by using the electron density based bond descriptors AIM,[11] NCI[12] and IGMH.[13] AIM analysis give rise to bond critical points between the metal–metal bond path for **2Pd** and **2Pt**, but is absent in case of the lighter **2Ni**. However, the electron density minimum found along the direct Ni–Ni axis (0.22 e $Å^{-3}$) is in line with the values found for the electron densities at the bcp for **2Pd** (0.26 e $Å^{-3}$) and **2Pt** (0.32 e $Å^{-3}$, Table S2, ESI†). These values are in the range found for other nickelophilic (0.18–0.36 e $Å^{-3}$),[14] palladophilic (0.21 e $Å^{-3}$)[15] and bimetallophilic interactions of the 6th period (0.28 e $Å^{-3}$).[16] The delocalization index δ(M|M) is also increasing from **2Ni** (0.17) over **2Pd** (0.26) to **2Pt** (0.37), indicating metallophilic interactions in all three metal species, with increasing strengths from Ni to Pt. This is further corroborated by inspection of the IGMH partitioning. Each metal atom is defined as an individual fragment and the interaction between the two fragments are depicted in Fig. 5, showing attractive blue colored areas between the metals which are increasing from Ni to Pt. The NCI approach is also capable to unravel the weak non-covalent metallophilic interactions, however in the present case it is more difficult to distinguish the metallophilic interactions from other inter- and intramolecular interactions (Fig. S11–S13, ESI†)[17] and therefore the IGMH method might be preferred in cases of weak interactions, being in the vicinity of other interactions.

The hydrogen-rich dimethylamine borane, Me_2NHBH_3, undergoes thermally induced dehydrogenation at 130 °C to give quantitatively the aminoborane $(Me_2NBH_2)_2$ comprising a four-membered ring structure.[18] While no reaction occurs below 100 °C, Manners *et al.* have shown that the dehydrogenation can be effectively catalyzed by addition of 0.5–5 mol% of [M(1,5-cod)(μ-Cl)]$_2$ (M = Rh, Ir; 1,5-cod = 1,5-cyclooctadiene) or $RhCl_3·3H_2O$ within 24 h at 45 °C or even lower temperatures at longer reaction times.[19,20] Bimetallic complexes offer interesting opportunities for catalytic reactions.[21] The interplay of two metal atoms in close proximity to each other often leads to cooperative effects and higher

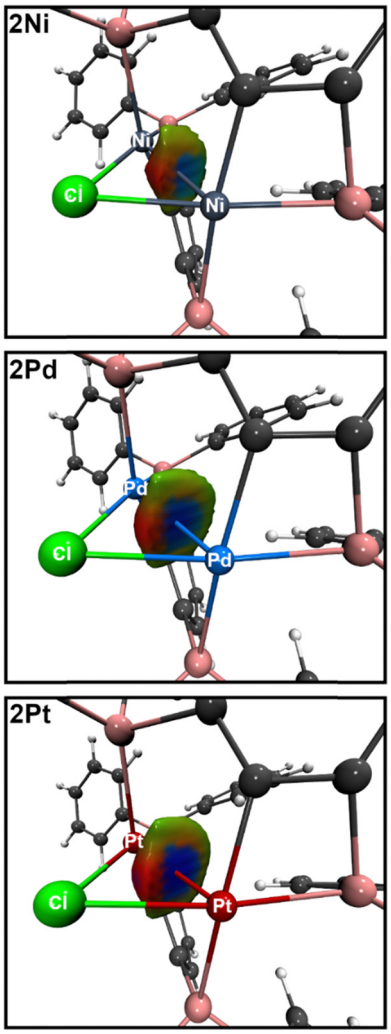

Fig. 5 IGM based on a Hirshfeld partition of the molecular density of **2M** (B3PW91/6-311+G(2df,p)). Each metal atom defines one fragment. IGMH isosurfaces at s(*r*) = 0.01 colour coded with sign(λ2)ρ in a.u. Blue surfaces refer to attractive forces and red to repulsive forces. Green indicates weak interactions.

activities compared to single site catalysts. In a first foray, we investigated the catalytic dehydrogenation of Me_2NHBH_3 at 70 °C.

Typically, NMR scale experiments with 4 mol% of **2Ni**, **2Pd** and **2Pt** were carried out in 1,2-difluorobenzene and the progress was monitored by recording ^{11}B NMR spectra. At the end of the reaction the spectrum showed almost exclusively a triplet centered at δ = 5.3 ppm with $^1J(^{11}B–^1H)$ coupling of 112 Hz that was unambiguously assigned to the cyclic $(Me_2NBH_2)_2$. The reaction proceeded three times faster upon using **2Ni** (6 h) than **2Pt** (18 h), whereas no reaction occurred in the presence of **2Pd** (Scheme 3). Approximate turnover frequencies were determined as TOF = 4.16 h^{-1} (**2Ni**) and 1.38 h^{-1} (**2Pt**). The ^{31}P NMR spectra of the reaction mixtures indicated that **2Ni** (δ = 26 ppm) and **2Pt** (δ = 29 ppm) changed into new yet unassigned species. In effort to further invest the kinetics of the dehydrogenation, the hydrogen gas evolution was monitored under the optimized reaction conditions for **2Ni** and **2Pt** (Fig. 6). The increase of the net pressure correlates well to the corresponding ^{11}B NMR data.

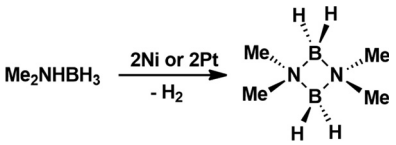

Scheme 3 Dehydrogenation of Me_2NHBH_3 catalysed by **2Ni** and **2Pt** in 1,2-difluorobenzene at 70 °C.

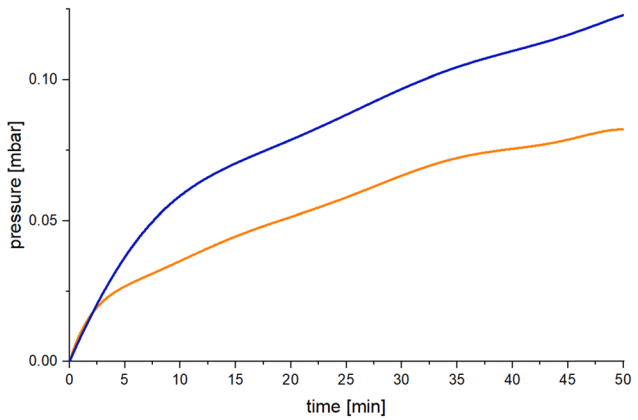

Fig. 6 Net pressure generation of the **2Ni** (blue) and **2Pt** (orange) catalyzed dehydrogenation of Me_2NHBH_3 in 1,2-difluorobenzene at 70 °C.

Again, **2Ni** shows three times faster reaction times than **2Pt**. After an initial sharp rise in pressure the reaction progressed approximately linear within the experiment. Notably, the use of **1**·$PtCl_2$ also drives the cyclization, but is very slow (96 h).

In summary, the reaction of $[2,6\text{-}(Ph_2P)_2C_6H_3]_2GaCl$ (**1**) with $Ni(dme)Cl_2$, $Pd(MeCN)_2Cl_2$ and $Pt(MeCN)_2Cl_2$, respectively, surprisingly proceeded with transmetallation and gave rise to the formation of cationic dinuclear group 10 complexes $[M_2(PCP)_2\mu\text{-}Cl][GaCl_4]$ (**2M**, M = Ni, Pd, Pt; PCP = $2,6\text{-}(Ph_2P)_2C_6H_3$)] featuring a rare series of attractive metallophilic interactions between group 10 elements.[22] The counterion $[GaCl_4]^-$ was formed from the expelled Ga atom of **1**. Only the reaction of **1** with $Pt(Et_2S)_2Cl_2$, afforded an expected Z-type complex, namely **1**·$PtCl_2$. The dehydrogenation of Me_2NHBH_3 to give $(Me_2NBH_2)_2$, is catalysed upon addition of **2Ni** and **2Pt**, whereas **2Pd** is inactive. Efforts are underway to broaden the scope of applications in catalysis and bond activation.

We are grateful to the Deutsche Forschungsgemeinschaft (DFG) for financial support. This work is dedicated to the memory of Professor Ian Manners.

Data availability

Spectroscopic and crystallographic data including figures of NMR spectra as well as the results of DFT calculations are given in the ESI.†

Conflicts of interest

There are no conflicts to declare.

Notes and references

1 M. A. Bennett, S. K. Bhargava, N. Mirzadeh and S. H. Priver, *Coord. Chem. Rev.*, 2018, **370**, 69–128.
2 M. Olaru, J. F. Kögel, E. Lork, S. Mebs, M. Vogt and J. Beckmann, *Chem. – Eur. J.*, 2020, **26**, 275–284.
3 (*a*) A. L. Balch, *Prog. Inorg. Chem.*, 1993, **41**, 239–329; (*b*) E. S. Smirnova, J. M. Muñoz Molina, A. Johnson, N. A. G. Bandeira, C. Bo and A. M. Echavarren, *Angew. Chem., Int. Ed.*, 2016, **55**, 7487–7491.
4 (*a*) M. Olaru, E. Rychagova, S. Ketkov, Y. Shynkarenko, S. Yakunin, M. V. Kovalenkoc, A. Yablonsiky, B. Andreev, J. Beckmann and M. Vogt, *J. Amer. Chem. Soc.*, 2020, **142**, 373–381; (*b*) G. Smolentsev, C. J. Milne, A. Guda, K. Haldrup, J. Szlachetko, N. Azzaroli, C. Cirelli, G. Knopp, R. Bohinc, S. Menzi, G. Pamfilidis, D. Gashi, M. Beck, A. Mozzanica, D. James, C. Bacellar, G. F. Mancini, A. Tereshchenko, V. Shapovalov, W. M. Kwiatek, J. Czapla-Masztafiak, A. Cannizzo, M. Gazzetto, M. Sander, M. Levantino, V. Kabanova, E. Rychagova, S. Ketkov, M. Olaru, J. Beckmann and M. Vogt, *Nat. Commun.*, 2020, **11**, 2131.
5 F. Meyer, T. Kuzmera, E. Lork, M. Vogt, J. Beckmann and Z. Allgem, *Anorg. Chem*, 2021, **647**, 1890–1895.
6 S. Furan, M. Molkenthin, K. Winkels, E. Lork, S. Mebs, E. Hupf and J. Beckmann, *Organometallics*, 2021, **40**, 3785–3796.
7 (*a*) P. Buchwalter, J. Rosé and P. Braunstein, *Chem. Rev.*, 2015, **115**, 28–126; (*b*) E. Lu and S. T. Liddle, *Group 10 Metal-Metal Bonds (Chapter 10) in Molecular Metal-Metal Bonds, Compounds, Synthesis, Properties*. ed. S. T. Liddle, Wiley-VCH, Weinheim, Germany, 2015, 325–395.
8 (*a*) P. Pyykkö, *Chem. Rev.*, 1997, **97**, 597–636; (*b*) H. Schmidbaur and A. Schier, *Chem. Soc. Rev.*, 2008, **37**, 1931–1951; (*c*) M. J. Katz, K. Sakai and D. B. Leznoff, *Chem. Soc. Rev.*, 2008, **37**, 1884–1895; (*d*) S. Sculfort and P. Braunstein, *Chem. Soc. Rev.*, 2011, **40**, 2741–2760; (*e*) H. Schmidbaur and A. Schier, *Chem. Soc. Rev.*, 2012, **41**, 370–412; (*f*) H. Schmidbaur and A. Schier, *Angew. Chem., Int. Ed.*, 2015, **54**, 746–784.
9 M. D. Risi, W. Henderson and G. C. Saunders, *Polyhedron*, 2024, **255**, 116992.
10 J. C. Hierso, *Chem. Rev.*, 2014, **114**, 4838–4867.
11 R. W. F. Bader, *Atoms molecules. a quantum theory*, Cambridge University Press, Oxford UK, 1991.
12 E. R. Johnson, S. Keinan, P. Mori-Sánchez, J. Contreras-García, A. J. Cohen and W. Yang, *J. Am. Chem. Soc.*, 2010, **132**, 6498–6506.
13 (*a*) C. Lefebvre, G. Rubez, H. Khartabil, J.-C. Boisson, J. Contreras-García and E. Hénon, *Phys. Chem. Chem. Phys.*, 2017, **19**, 17928–17936; (*b*) T. Lu, *J. Comput. Chem.*, 2022, **43**, 539–555.
14 A. S. Novikov, *Inorg. Chim. Acta*, 2018, **483**, 21–25.
15 S. Furan, E. Lork, S. Mebs, E. Hupf and J. Beckmann, *Z. Anorg. Allg. Chem.*, 2020, **646**, 856–865.
16 R. Gericke, M. A. Bennett, S. H. Privér and S. K. Bhargava, *Inorg. Chem.*, 2023, **62**, 8846–8862.
17 S. Furan, M. Vogt, K. Winkels, E. Lork, S. Mebs, E. Hupf and J. Beckmann, *Organometallics*, 2021, **40**, 1284–1295.
18 A. B. Burg and C. L. Randolph, *J. Am. Chem. Soc.*, 1949, **71**, 3451–3455.
19 C. A. Jaska, K. Temple, A. J. Lough and I. Manners, *Chem. Commun.*, 2001, 962–963.
20 C. A. Jaska, K. Temple, A. J. Lough and I. Manners, *J. Am. Chem. Soc.*, 2003, **125**, 9424–9434.
21 (*a*) J. Campos, *Nat. Rev. Chem.*, 2020, **4**, 696–702; (*b*) M. Navarro, J. J. Moreno, M. Peréz-Jiménez and J. Campos, *Chem. Commun.*, 2022, **58**, 11220–11235.
22 O. Zheng, S. Borsley, G. S. Nichol, F. Duarte and S. L. Cockroft, *Angew. Chem., Int. Ed.*, 2019, **131**, 12747–12753.